Research Square

Preprints are preliminary reports that have not undergone peer review.
They should not be considered conclusive, used to inform clinical practice,
or referenced by the media as validated information.

Integrative CRISPR-Cas9 Screening Reveals Lethal Genes Driving Metastasis and Prognosis in Prostate Adenocarcinoma

Yuxin Xie
Tianjin Medical University
Shuo Wang
Tianjin Medical University
Yukui Gao
gaoyukui@wnmc.edu.cn

The First Affiliated Hospital of Wannan Medical College, Yijishan Hospital

Research Article

Keywords: Prostate adenocarcinoma, CRISPR-Cas9, bulk-RNA sequencing, prognosis, tumor dependency

Posted Date: March 5th, 2026

DOI: https://doi.org/10.21203/rs.3.rs-8953080/v1

License: This work is licensed under a Creative Commons Attribution 4.0 International License.
Read Full License

Additional Declarations: No competing interests reported.

Integrative CRISPR-Cas9 Screening Reveals Lethal Genes Driving Metastasis and Prognosis in Prostate Adenocarcinoma

Yuxin Xie[23#],Shuo Wang[4#],Yukui Gao[1*]

[1]Department of Urology, The First Affiliated Hospital of Wannan Medical College, Yijishan Hospital, Wuhu 241001, Anhui, People’s Republic of China.
[2]Tianjin Institute of Urology, The Second Hospital of Tianjin Medical University, Tianjin, People's Republic of China.
[3]Department of Urology, The Second Hospital of Tianjin Medical University, Tianjin, People's Republic of China.
[4]Department of Respiratory and Critical Care Medicine, Tianjin Medical University General Hospital, Tianjin, 300052, China.
[#] These authors contributed equally to this work.

* Corresponding author:

Dr.Yukui Gao,Department of Urology, The First Affiliated Hospital of Wannan Medical College, Yijishan Hospital, Wuhu 241001, Anhui, China.E-mail:gaoyukui@wnmc.edu.cn

Abstract
Prostate adenocarcinoma (PRAD) has become one of the most prevalent malignancies in men worldwide. Although advances in diagnostic techniques and targeted therapies have improved clinical outcomes, a significant subset of patients still develops aggressive, metastatic disease with limited treatment options. At present, identifying reliable biomarkers for early risk stratification remains a critical unmet need in prostate cancer research.This study established a novel genetic signature through multi-omics integration to enhance risk stratification and identify therapeutic targets.Integrated analysis of CRISPR-Cas9 screening and bulk RNA sequencing data identified tumor-dependent genes essential for PRAD cell viability.Pathway enrichment analysis demonstrated critical involvement of these genes in cell cycle regulation and tumor progression.An 11-gene prognostic signature was constructed via LASSO regression, effectively stratifying patients into distinct low-risk and high-risk cohorts.The high-risk cohort demonstrated significantly reduced progression-free survival (PFS; log-rank $p<0.001$).Among the hub genes identified, CDC45 exhibited marked upregulation in tumor tissues, which was confirmed by both Western blotting and qRT-PCR. Subsequent functional interrogation established CDC45 as a key driver of tumor proliferation. Collectively, this study not only establishes a robust prognostic signature for PRAD but also nominates CDC45 as a promising therapeutic target, thereby advancing precision oncology strategies.
Keywords: Prostate adenocarcinoma, CRISPR-Cas9, bulk-RNA sequencing, prognosis,tumor dependency

Introduction

prostate cancer (PCa) represents the second most common cancer diagnosis in males and ranks as the fifth primary contributor to mortality among all cancer types.[1, 2].Although radical prostatectomy remains the standard treatment for localized disease, approximately 25–30% of patients progress to metastatic stages within 10 years, with a five-year survival rate of less than 30%[3]. These outcomes highlight the critical need to identify novel therapeutic targets that underpin tumor progression at the molecular level.

The CRISPR-Cas9 system has revolutionized functional genomics by enabling high-throughput, genome-wide screens of gene essentiality through Cas9-sgRNA–mediated DNA targeting[4, 5].To identify genes critical for cancer cell fitness, we leveraged data from the Cancer Dependency Map (DepMap). This consortium integrates genome-scale CRISPR knockout screens across hundreds of genetically diverse cancer cell lines to systematically identify genetic dependencies—genes whose loss of function selectively impairs cell proliferation or survival. This resource was instrumental in pinpointing candidate oncology targets [6].Genes identified through CRISPR screening possess considerable potential for translational applications.Analysis of DepMap CRISPR-Cas9 data by Xiao et al. revealed that upregulation of NLRP4 confers resistance to olaparib in pancreatic cancer[7].Similarly, Wang et al. employed genome-wide CRISPR screening to identify seven genes critically linked to breast cancer cell proliferation[8]. These

findings underscore the utility of the DepMap resource in guiding precision oncology strategies. Cross-validation with databases such as TCGA can further enhance the clinical relevance of identified targets.To systematically uncover genes essential for prostate adenocarcinoma (PRAD) cell survival, Through the integration of genome-wide CRISPR-Cas9 loss-of-function screens and RNA-seq datasets from The Cancer Genome Atlas(TCGA), we discovered 11 genes that are essential for tumor cell viability.(dependency score < –0.5). This approach allows precise identification of genetic vulnerabilities associated with metastatic potential.

Among the top candidates, cell division cycle protein 45 (CDC45) emerged as a critical regulator due to its dual role in maintaining genomic integrity and driving oncogenesis,and initiates DNA replication through interaction with replication protein A (RPA)[9].CDC45 demonstrates pan-cancer dysregulation, exhibiting significant associations with tumorigenesis, malignant progression, and clinical prognosis across diverse malignancies[10-13]. However, its role in regulating prostate cancer stemness and metastasis remains poorly characterized.

To address these gaps, we integrated CRISPR screening with multi-omics analyses to pursue three major objectives:1.Develop a metastasis-associated gene signature using machine learning to prioritize clinically actionable targets;2.Evaluate the diagnostic and prognostic value of CDC45 across PRAD clinical cohorts;3.Investigate CDC45's immunomodulatory roles via tumor microenvironment deconvolution and immune cell interaction mapping.

This integrative strategy bridges functional genomics with clinical informatics, revealing CDC45 as a central regulator of tumor progression in prostate cancer.

Materials and Methods

Data acquisition and preprocessing

Gene expression profiles (FPKM values) and corresponding clinical data for a discovery cohort of 554 prostate cancer patients were retrieved from The Cancer Genome Atlas (TCGA) database (https://www.cancer.gov/tcga).

CRISPR-Cas9 screening and identification of essential genes

To identify genes essential for prostate cancer cell survival, we utilized the CRISPR-Cas9/CERES (Copy-number-adjusted Essentiality Ranking Evaluation System) analytical pipeline. CERES minimizes false-positive results arising from copy number variations in CRISPR–Cas9 essentiality screens. We obtained CERES dependency scores for 12 primary prostate cancer cell lines (MDAPCA2B, WPE1NA22, P4E6, SHMAC4, SHMAC5, PC3, VCAP, NCIH660, 22RV1, DU-145CLONEFGC, DU145, PWR1E, and BPH1) screened with the Avana sgRNA library from the DepMap database. The gene effect score represents cell dependency; a lower score indicates higher essentiality. Candidate proliferation-associated genes were identified based on two criteria: (1) a CERES score < -1 in at least 75% of the analyzed cell lines; and (2) a mean CERES score < -1 across all 12 cell lines.

Differential expression analysis

Differentially expressed genes (DEGs) between tumor and normal tissues were identified using the "DESeq2" R package. Genes with an adjusted p-value < 0.05 and an absolute fold-change > 1 were considered statistically significant. The previously identified essential genes were intersected with DEGs: growth-inhibitory genes were overlapped with downregulated DEGs, while growth-promoting genes were intersected with upregulated DEGs. The study workflow is illustrated in Fig. 1.

Construction of the prognostic signature

A prognostic model was constructed using Least Absolute Shrinkage and Selection Operator (LASSO) Cox regression analysis via the glmnet R package. The optimal penalty parameter (λ) was determined by 10-fold cross-validation (lambda.min), resulting in a signature of 11 genes with non-zero coefficients. Risk scores were calculated for each patient, and the TCGA-PRAD cohort was stratified into high- and low-risk groups based on the median risk score. Survival differences were assessed using Kaplan-Meier curves and the log-rank test. The predictive accuracy of the model was evaluated using time-dependent receiver operating characteristic (ROC) analysis via the timeROC package.

Weighted Gene Co-expression Network Analysis (WGCNA)

A weighted co-expression network was constructed using the WGCNA R package (v1.71) based on tumor sample expression data from the TCGA-PRAD cohort. After excluding outlier samples, a soft-thresholding power of $\beta = 10$ was selected to ensure a scale-free network topology ($R^2 > 0.9$). The adjacency matrix was transformed into a topological overlap matrix (TOM) to minimize noise. Modules were identified using hierarchical clustering with a dynamic tree cut algorithm (minimum module size = 100). Similar modules were merged using a cut height of 0.3.

Functional enrichment and interaction network analysis

Gene Ontology (GO) and Kyoto Encyclopedia of Genes and Genomes (KEGG) pathway enrichment analyses were performed using the clusterProfiler R package (version 4.2.2). Pathways with a p-value < 0.05 and q-value < 0.05 were considered significantly enriched. The protein-protein interaction (PPI) network and functional associations of the 11-gene signature were analyzed using the GeneMANIA database.

Cell culture

Human prostate cancer cell lines were obtained from Procell Life Science & Technology Co., Ltd. Cells were cultured in RPMI-1640 medium (Procell) supplemented with 10% fetal bovine serum (FBS) at 37 °C in a 5% CO_2 humidified atmosphere. Cell line identities were verified via Short Tandem Repeat (STR) profiling, and routine testing confirmed the absence of mycoplasma contamination.

siRNA transfection

Three distinct siRNA sequences targeting the CDC45 gene were designed according

to the full-length cDNA sequence of CDC45 (GenBank accession number: NM_001178010.2). All siRNA constructs were synthesized by Beijing Wengene Co., Ltd. (Beijing, China).

RNA isolation and quantitative Real-Time PCR (qRT-PCR)

Total RNA was extracted using TRIzol™ reagent and reverse-transcribed into cDNA using the AG® Evo M-MLV RT Kit with gDNA Clean (Accurate Biology). qRT-PCR was performed using SYBR Green qPCR Master Mix on a real-time PCR system. Relative expression levels were calculated using the $2^{-\Delta\Delta Ct}$ method, with GAPDH serving as the endogenous control. The primer sequences were:GAPDH Forward: 5′-GGAAGCTTGTCATCAATGGAAATC-3′GAPDH Reverse: 5′-TGATGACCCTTTTGGCTCCC-3′CDC45 Forward: 5′-AGGATGGCTCAGGGACAGAT-3′CDC45 Reverse: 5′-GCCGGTTCTTTGTCGAACAC-3′

Western blot analysis

Total protein was extracted using RIPA lysis buffer, separated by SDS-PAGE, and transferred onto PVDF membranes. Membranes were blocked and incubated overnight at 4 °C with primary antibodies against CDC45 (1:1,000, Abcam, ab126762) and GAPDH (1:50,000, Proteintech, 60004-1-Ig). After incubation with HRP-conjugated secondary antibodies, protein bands were visualized using an enhanced chemiluminescence (ECL) system.

Transwell invasion assay

Cell invasion was assessed using Transwell chambers (8 μm pore size) pre-coated with Matrigel. Cells ($2*10^4$) in serum-free medium were plated in the upper chamber, while medium containing 10% FBS was added to the lower chamber. After 24 hours, non-invading cells were removed. Invaded cells on the lower surface were fixed with 4% paraformaldehyde, stained with 0.1% crystal violet, and imaged. The number of invaded cells was quantified by counting five randomly selected fields per well.

Wound healing assay

PC3 and DU-145 cells were seeded in 6-well plates and grown to confluence. A linear scratch was created using a sterile 200 μL pipette tip. Cells were washed with PBS to remove debris and cultured in serum-free medium to minimize the effect of cell proliferation. Images were captured at 0 h and 48 h post-wounding using an inverted microscope. Wound closure was quantified using ImageJ software.

Statistical analysis

All statistical analyses were performed using R software (version 4.2.1). Differences between groups were compared using the Student’s t-test or Wilcoxon test for continuous variables, as appropriate. Survival differences were analyzed using the log-rank test. A two-sided p-value < 0.05 was considered statistically significant.

Results

Determination of Functional Genomic Genes in Prostate Adenocarcinoma

To identify functionally significant genes in prostate adenocarcinoma (PRAD), we performed an integrative analysis combining transcriptomic data and CRISPR-based functional genomics. Differential gene expression analysis using the TCGA-PRAD dataset yielded the top 10 differentially expressed genes (DEGs), visualized via a volcano plot (Fig. 2A).

To assess the essentiality of these genes, we conducted pooled CRISPR-Cas9 screens across 12 PRAD cell lines, calculating gene dependency scores. Genes with consistent dependency scores below –0.5 across all cell lines were considered essential for cell survival. Intersecting these essential genes with metastasis-associated DEGs from TCGA analysis produced a refined list of 27 high-confidence candidates (Fig. 2B), which we visualized in an integrated heatmap (Fig. 2C).

To further explore the biological functions of these genes, functional enrichment analysis was subsequently carried out. KEGG pathway analysis revealed significant enrichment in pathways related to cell cycle regulation, p53 signaling, and cellular senescence (Fig. 2D), implicating their role in tumor progression. GO analysis further identified key biological processes such as nuclear division and cell cycle control (Fig. 2E), underscoring the functional relevance of the candidate genes in PRAD pathogenesis.

Construction of the MGG-Related Risk Model

To develop a prognostic model using metastasis-associated genomic genes (MGGs), univariate Cox regression analysis was first carried out on TCGA-PRAD samples (Fig. 3A).To optimize the prognostic model, we applied LASSO Cox regression to the 27 candidate genes, which yielded an 11-gene risk signature comprising: ATP6V0C, BOP1, CDC20, CDC45, PABPN1, PLK1, RPL26, RPS1, RRM2, SPC24, and SPOUT1 (Fig. 3B, C). Based on the median risk score derived from the model, patients were stratified into high- and low-risk groups (Fig. 3D). This risk stratification effectively distinguished patients with progressive disease from those with stable outcomes, with the high-risk group showing significantly poorer clinical outcomes (Fig. 3E).

To further assess the model's prognostic relevance, Kaplan–Meier analysis of progression-free interval (PFI) demonstrated markedly worse survival in the high-risk group (Fig. 3F). A prognostic nomogram incorporating the risk score and key clinicopathological variables was developed to predict progression-free interval (PFI) probabilities at 1, 3, and 5 years(Fig. 3G). The model exhibited robust predictive accuracy, as evidenced by time-dependent ROC curves with area under the curve (AUC) values consistently above 0.75 (Fig. 3H), indicating strong discriminatory capability for progression risk.

WGCNA Identifies CDC45 as a Hub Gene in Prostate Adenocarcinoma

To identify key regulators of tumor progression in prostate adenocarcinoma, we

performed weighted gene co-expression network analysis (WGCNA) on transcriptomic data from the TCGA-PRAD cohort. A soft-thresholding power of 3 was selected to ensure scale-free network topology (Fig. 4A). Hierarchical clustering and dynamic tree cutting identified 12 distinct gene modules at a cut height of 0.3 (Fig. 4B).

Among these, the red module showed the strongest positive correlation with tumor progression (correlation coefficient = 0.46, $p < 0.001$) (Fig. 4C). This module was notably enriched for five metastasis-associated genomic genes (MGGs): CDC45, CDC20, RRM2, PLK1, and SPC24 (Fig. 4D). Of these, CDC45 emerged as the most prognostically relevant hub gene, with a 1-year progression prediction AUC of 0.696 (Fig. 4E–I), suggesting its potential as a biomarker for early disease progression.

CDC45 as a Key Prognostic and Predictive Marker in PRAD

Compared to normal prostate tissues, CDC45 expression showed marked upregulation in prostate cancer (PCa) samples($p < 0.001$; Fig. 5A). Elevated CDC45 levels were significantly associated with advanced nodal metastasis (N-stage) and higher Gleason scores, indicating a link with tumor aggressiveness (Fig. 5B–C).The prognostic value of CDC45 was further substantiated by time-dependent ROC analyses, yielding AUC values above 0.70 for 1-, 3-, and 5-year progression-free interval (PFI) predictions (Fig. 5D). Protein–protein interaction (PPI) network analysis using GeneMANIA highlighted CDC45's central role in DNA replication and cell cycle regulation (Fig. 5E).GO enrichment analysis confirmed that CDC45 participates in key biological processes, including DNA replication initiation, G1/S phase transition, and nuclear DNA replication (Fig. 5F). Moreover, CDC45 expression positively correlated with the activity of DNA repair and replication-related pathways (Fig. 5G–H), implicating its role in maintaining—or dysregulating—genomic stability.

Taken together, these findings underscore CDC45 as a potential oncogenic driver and robust biomarker of poor prognosis in PRAD, particularly through its involvement in replication stress and proliferative signaling.

CDC45 Modulates Immune Infiltration in Prostate Adenocarcinoma

To investigate the immunomodulatory function of CDC45, we conducted CIBERSORT analysis on transcriptomic data from 499 PRAD samples. Based on the median CDC45 expression level, patients were stratified into high-expression and low-expression groups, and immune infiltration across 22 immune cell subsets was profiled (Fig. 6A).

A significant association was observed between high CDC45 expression and an increased density of tumor-promoting immune cells, notably activated B cells, mast cells, NK cells, and Th17 cells. In contrast, low CDC45 expression correlated with elevated levels of tumor-suppressive immune subsets, such as $CD4^+$ cytotoxic T cells and γδ T cells ($p < 0.001$; Fig. 6B).

Notably, CDC45 expression exhibited a positive correlation with regulatory T cell (Treg) abundance ($p < 0.05$; Fig. 6C), while an inverse relationship was observed with $CD8^+$ cytotoxic T cell infiltration ($p < 0.05$; Fig. 6D). Furthermore, patients in the

high-CDC45 group demonstrated significantly higher Tumor Immune Dysfunction and Exclusion (TIDE) scores ($p < 0.01$; Fig. 6E), suggesting enhanced immune evasion capacity.These results implicate CDC45 as a modulator of immune cell composition in the tumor microenvironment, promoting immune suppression and potentially contributing to resistance to immunotherapy in prostate adenocarcinoma.

CDC45 Knockdown Impairs Tumor Aggressiveness In Vitro

To elucidate CDC45's function, we performed siRNA-mediated knockdown in PC-3 and DU-145 prostate cancer cells. The efficiency of CDC45 silencing was rigorously validated at the transcriptional and translational levels by qRT-PCR and Western blot analysis, respectively (Fig. 7A, B), both showing a substantial reduction in expression.Functional assays revealed that CDC45 knockdown markedly reduced colony-forming ability in both cell lines, as evidenced by fewer and smaller colonies compared to the control group (Fig. 7C), suggesting decreased proliferative and tumorigenic potential. The impact on cell motility was further evaluated using scratch wound healing and transwell migration assays.CDC45-silenced cells exhibited significantly impaired migration capacity in both PC-3 and DU-145 lines compared to negative control siRNA-transfected cells (Figs. 7D–E and 7F–G).

Collectively, these results indicate that CDC45 promotes tumor aggressiveness in prostate cancer cells by enhancing both proliferative and migratory capacities.

Discussion

In this study, we identified five metastasis-associated genes—CDC45, CDC20, RRM2, PLK1, and SPC24—as key regulators of tumor proliferation and metastatic spread in prostate adenocarcinoma (PRAD). Among them, CDC45 emerged as a central node, essential for DNA replication fidelity via its role in the CMG (CDC45–MCM–GINS) helicase complex.This evolutionarily conserved replication machinery unwinds double-stranded DNA, stabilizes replication forks, and ensures high-fidelity genome duplication [17].

CDC45 overexpression disrupts replication timing control, a mechanism linked to chromosomal instability and oncogenic proliferation across multiple cancers, including cervical ,colorectal , and ovarian[18-20]. In PRAD,Our analysis revealed a significant upregulation of CDC45 expression, which was confirmed at both the transcriptional (mRNA) and translational (protein) levels. This upregulation was associated with high diagnostic accuracy and poor clinical outcomes,consistent with findings in gastric and colorectal cancers[13, 21] . These results highlight CDC45's pan-cancer significance as a biomarker and driver of replication stress.

Functionally, CDC45 knockdown in PC-3 and DU-145 cell lines reduced colony formation and impaired migratory capacity, confirming its role in sustaining tumor aggressiveness. Beyond proliferation, our immune profiling revealed a dual role for CDC45 in shaping an immunosuppressive tumor microenvironment (TME). CDC45 expression correlated with the infiltration of myeloid-derived suppressor cells

(MDSCs), B cells, mast cells, NK cells, and Th17 cells[22].In contrast, low CDC45 expression was associated with increased infiltration of activated $CD4^+$ T cells and γδ T cells—effectors critical for immune surveillance of early metastases. CDC45's negative association with $CD8^+$ T cells and positive correlation with regulatory T cells (Tregs) further supports its role in immune evasion. These findings were reinforced by elevated TIDE scores in CDC45-high tumors, predicting resistance to immune checkpoint blockade therapy. We propose that CDC45 fosters a "cold" TME by recruiting immunosuppressive cells via CXCL12/CXCR4 chemotaxis, promoting PD-L1 upregulation, and exhausting cytotoxic T cell function.

Despite these findings, several limitations warrant consideration:1.Functional validation of bioinformatic predictions via CDC45 overexpression in castration-resistant, androgen-deprived PDX models is needed.2.Preclinical studies are required to evaluate CDC45 inhibition in combination with anti-PD-1 therapy, addressing TME-driven resistance.Future efforts using spatial transcriptomics, CRISPR screens, and single-cell profiling may uncover context-specific CDC45 functions and inform biomarker-driven clinical trials targeting metastatic PRAD.

Data Availability Statement

Publicly available datasets were analyzed in this study. The TCGA-PRAD RNA-seq data can be found in the UCSC Xena browser at: https://xenabrowser.net/datapages/?dataset=TCGA-PRAD.star_fpkm.tsv&host=https%3A%2F%2Fgdc.xenahubs.net&removeHub=https%3A%2F%2Fxena.treehouse.gi.ucsc.edu%3A443. The CRISPR-Cas9 screening data were obtained from the Dependency Map (DepMap) portal and can be accessed at:https://depmap.org/

Clinical trial number

not applicable.

Funding

This work was supported by Anhui Provincial Special Fund for Translational Research in Clinical Medicine(202204295107020011) and The First Affiliated Hospital of Wannan Medical College Special Fund for Talent Introduction (KY28880624).

Consent for publication

Not Applicable.

Competing Interests

The authors have declared that no competing interest exists.

Author Contributions

XYX,WS and GYK designed the study and collected research data.XYX analyzed the data and designed the experiments.WS wrote the manuscript.GYK conducted experiments and organized the data .

Ethics Approval and Consent to participate

Not applicable.

Figure legends

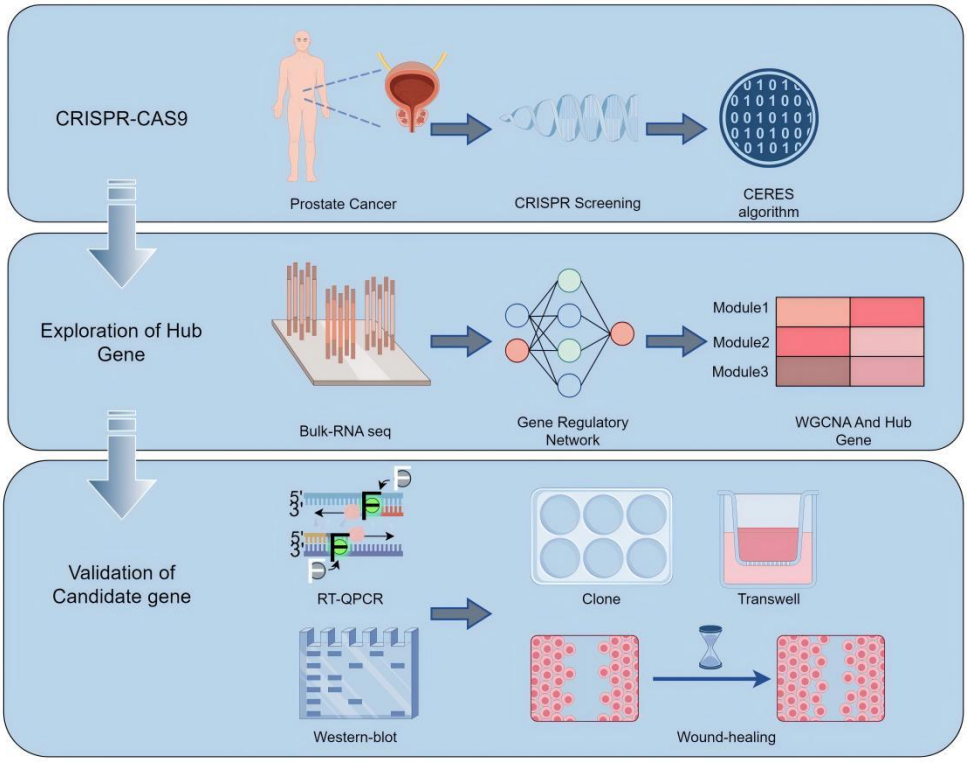


Figure 1 Schematic design of the study.

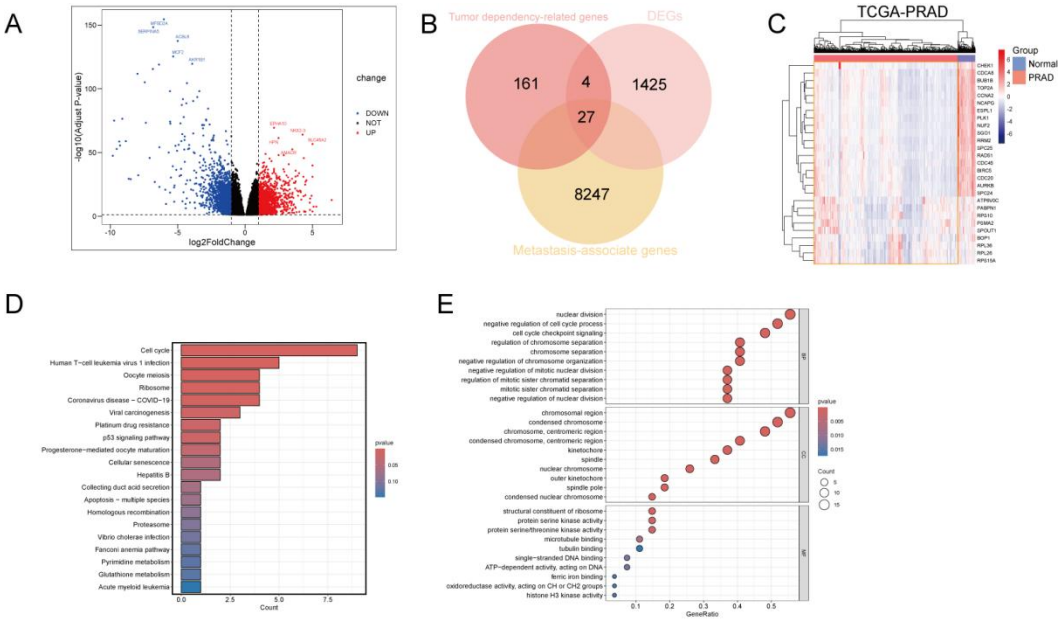


Figure 2 Identification of oncogenic genes using integrated TCGA and DepMap datasets. (A) Volcano plot of differentially expressed genes (DEGs) between PRAD

tumors and normal prostate tissues. **(B)** Venn diagram intersecting DEGs, growth promoting genes, and metastasis-associated genes. **(C)** Heatmap illustrating the expression levels of candidate oncogenes in the TCGA-PRAD dataset. **(D)** KEGG pathway enrichment analysis of candidate oncogenes. **(E)** GO enrichment bubble plot of candidate oncogenes.

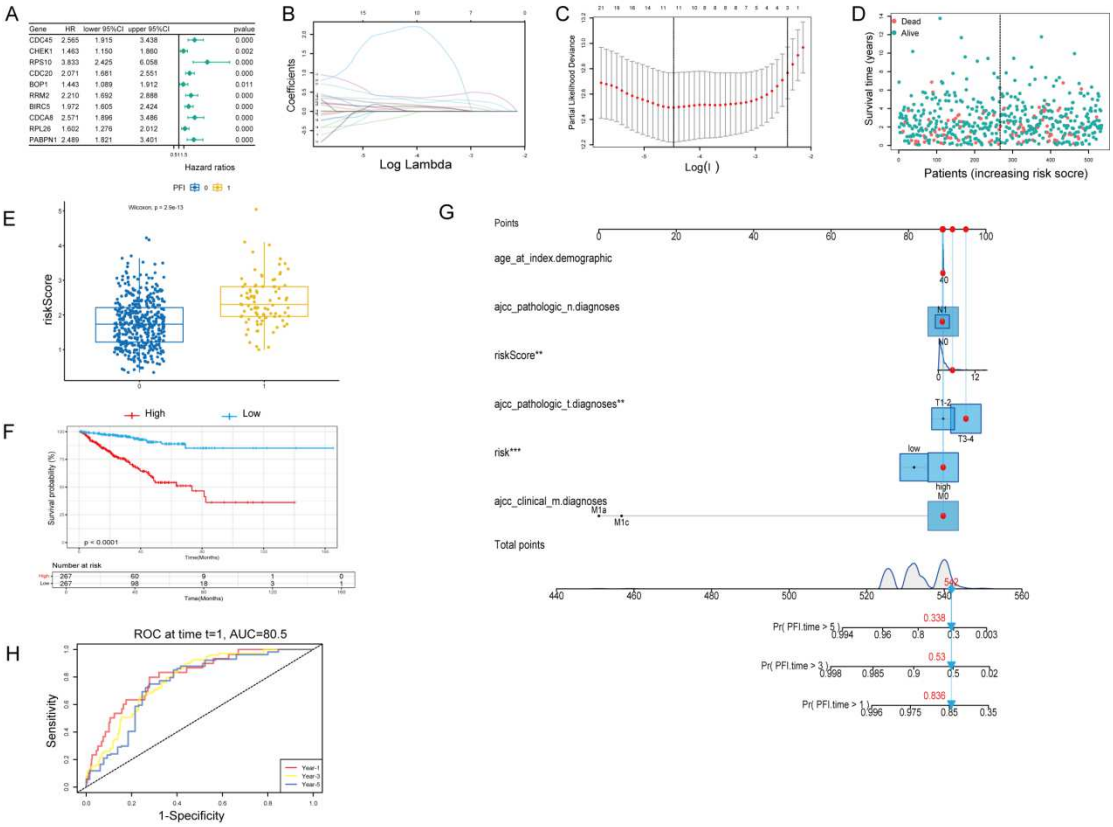


Figure 3 LASSO-based prognostic modeling of candidate genes in TCGA-PRAD cohort. (A) Univariate Cox regression results for candidate genes presented as a forest plot. **(B)** Selection of the optimal penalty parameter (λ) based on minimization of partial likelihood deviance. **(C)** Coefficient profiles of candidate genes derived from the LASSO regression analysis. **(D)** Distribution of patient vital status according to risk score stratification. **(E)** Comparison of risk scores between patients with and without disease progression. **(F)** Kaplan-Meier analysis of PFS between low-risk and high-risk groups. **(G)** Nomogram developed for predicting progression-free interval (PFI) in the TCGA-PRAD cohort. **(H)** Time-dependent ROC curves evaluating the predictive performance of the risk score.

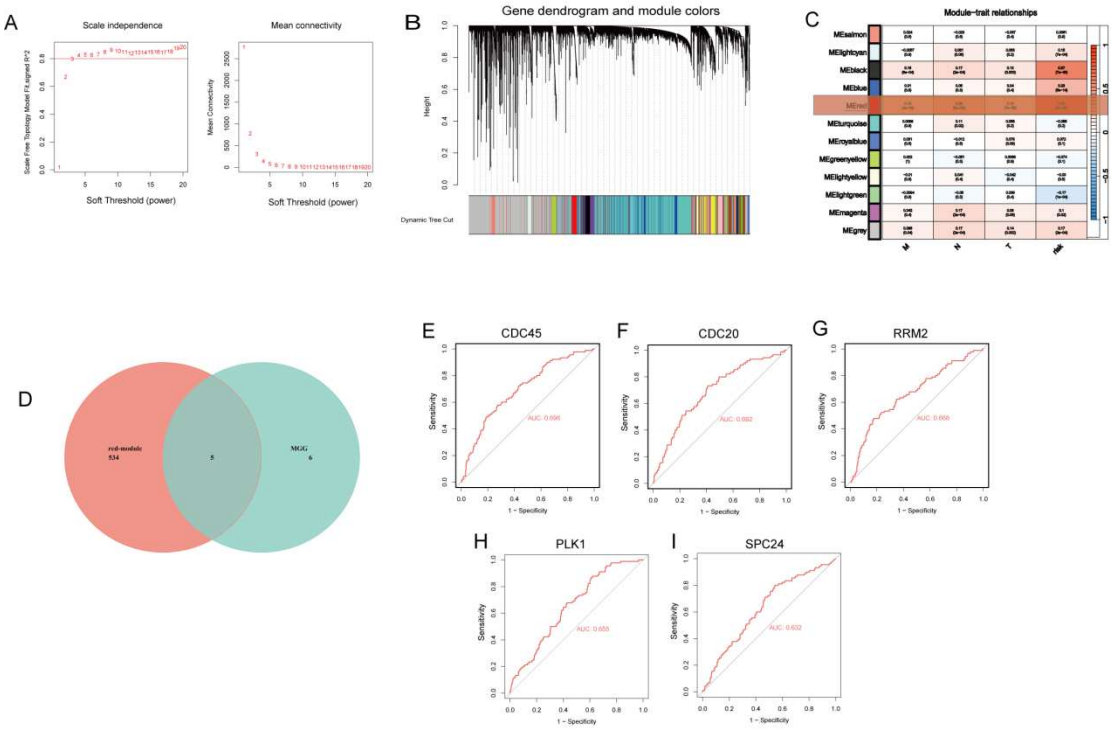


Figure 4 Hub gene identification through WGCNA in TCGA-PRAD. (A) Analysis of scale-free fit index for soft-thresholding power selection. **(B)** Identification of gene co-expression modules using WGCNA. **(C)** Module-trait association heatmap correlating co-expression modules with progression-free survival. **(D)** Intersection of 11 prognostic signature genes and key WGCNA modules. **(E-I)** ROC curves evaluating diagnostic potential of hub genes in TCGA-PRAD.

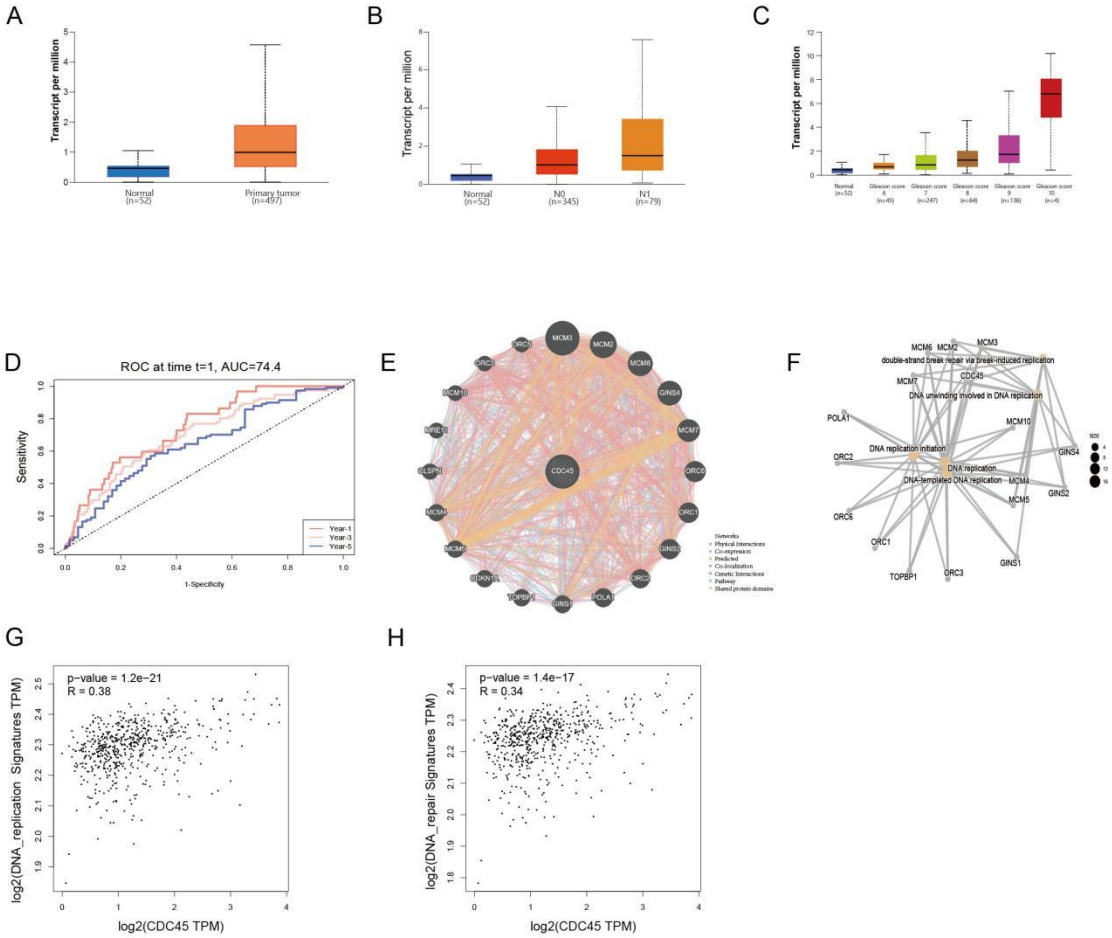


Figure 5 Evaluation of CDC45 as a Combined Diagnostic and Prognostic Indicator in Prostate Cancer. (A) Differential CDC45 mRNA expression in TCGA-PRAD tumors versus normal prostate tissues. **(B)** Association of CDC45 expression with pathological nodal (pN) stage. **(C)** Correlation between CDC45 expression and Gleason score. **(D)** Time-dependent ROC analysis of CDC45's prognostic capacity. （ **E** ） Protein-protein interaction network generated by GeneMANIA.（**F**） GO enrichment analysis of genes co-expressed with CDC45. **(G-H)** Association between CDC45 expression and cell cycle pathway.

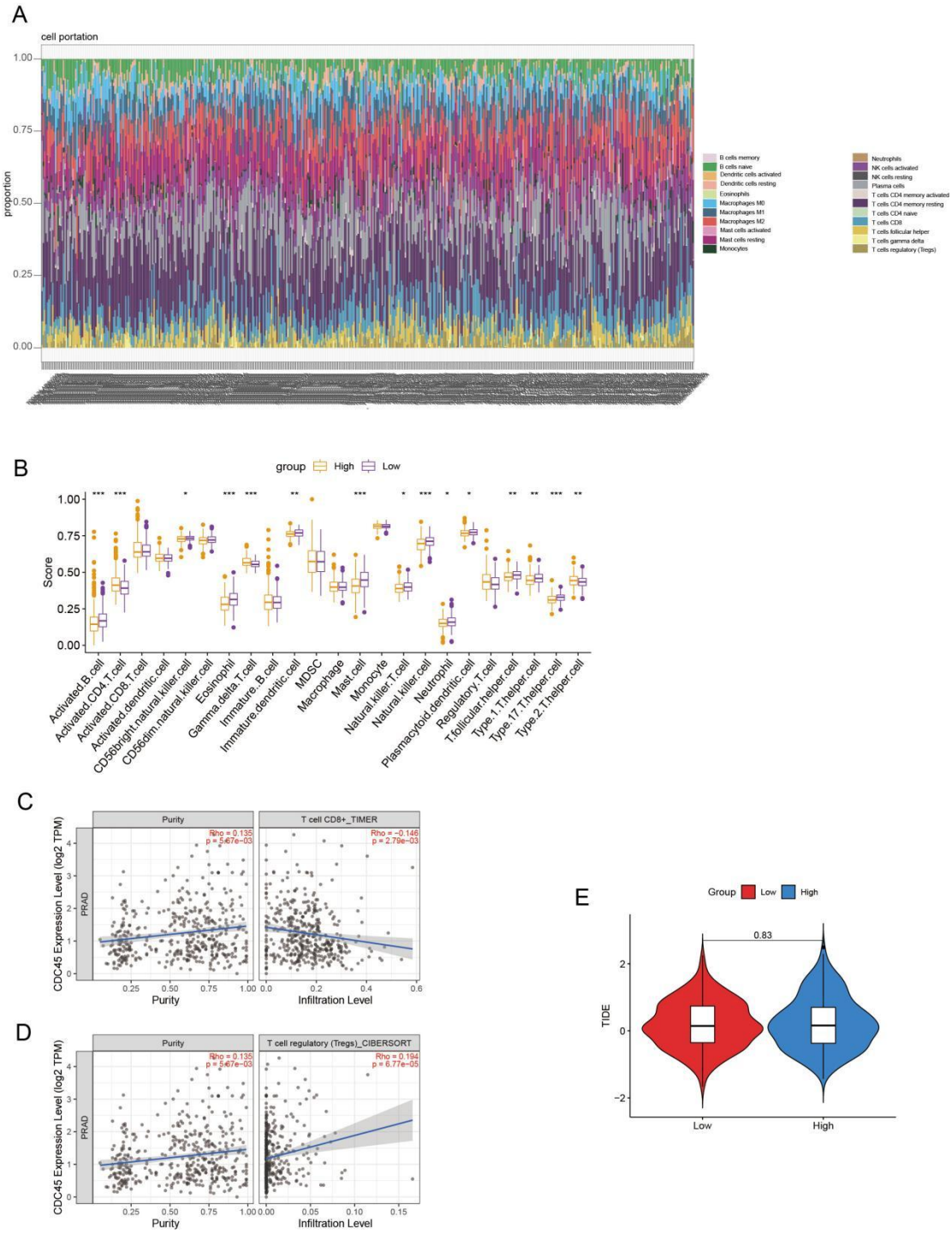


Figure 6 Association of CDC45 expression with tumor-infiltrating immune cells in prostate adenocarcinoma. (A) Relative abundance of 22 immune cell types across TCGA-PRAD specimens. **(B)** Differential immune cell infiltration quantified by CIBERSORTx in low- versus high-CDC45 expression groups. **(C-D)** Scatter plots demonstrating significant correlations between CDC45 expression and selected immune cell populations. **(E)** Comparative TIDE scores stratified by CDC45 expression levels.

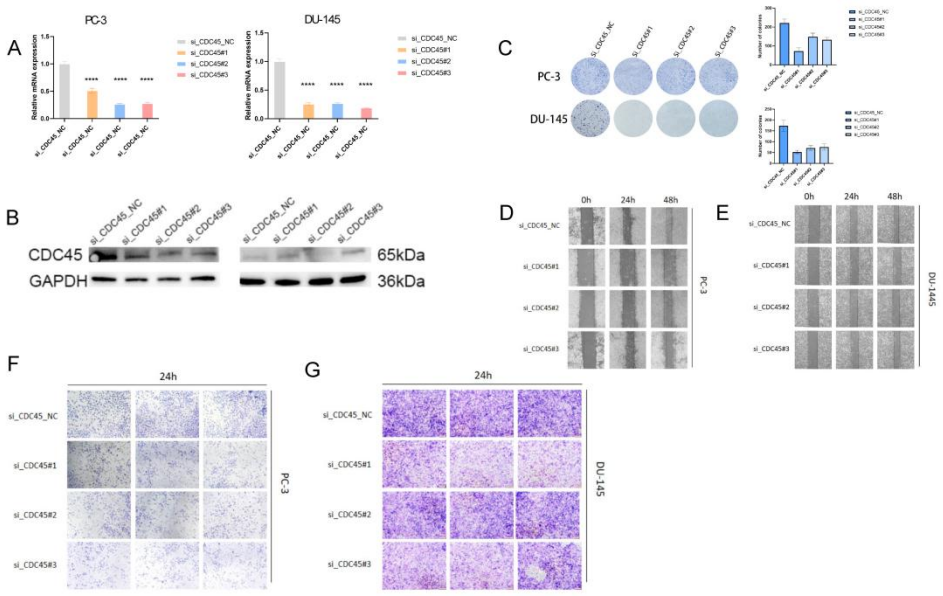


Figure 7 Functional validation of CDC45 in prostate cancer progression. (A) qPCR quantification of CDC45 mRNA knockdown efficiency. **(B)** Western blot verification of CDC45 protein depletion. **(C)** Colony formation assay demonstrating proliferative capacity impairment. **(D-E)** Wound healing assays quantifying migration inhibition. **(F-G)** Transwell migration assays assessing invasive potential reduction.

References

1. Bergengren O, Pekala KR, Matsoukas K, Fainberg J, Mungovan SF, Bratt O, et al. 2022 Update on Prostate Cancer Epidemiology and Risk Factors-A Systematic Review. Eur Urol. 2023; 84: 191–206.

2. Sung H, Ferlay J, Siegel RL, Laversanne M, Soerjomataram I, Jemal A, et al. Global Cancer Statistics 2020: GLOBOCAN Estimates of Incidence and Mortality Worldwide for 36 Cancers in 185 Countries. CA Cancer J Clin. 2021; 71: 209–49.

3. Valdez-Vargas AD, Sánchez-López HM, Badillo-Santoyo MA, Maldonado-Valadez RE, Manzo-Pérez BO, Pérez-Abarca VM, et al. Recurrence rate of localized prostate cancer after radical prostatectomy according to D'amico risk classification in a tertiary referral hospital: association study. Cir Cir. 2021; 89: 520–7.

4. Usman B, Nawaz G, Zhao N, Liao S, Qin B, Liu F, et al. Programmed Editing of Rice (Oryza sativa L.) OsSPL16 Gene Using CRISPR/Cas9 Improves Grain Yield by Modulating the Expression of Pyruvate Enzymes and Cell Cycle Proteins. Int J Mol Sci. 2020; 22.

5. Louradour I, Ghosh K, Inbar E, Sacks DL. CRISPR/Cas9 Mutagenesis in Phlebotomus papatasi: the Immune Deficiency Pathway Impacts Vector Competence for Leishmania major. mBio. 2019; 10.

6. Arafeh R, Shibue T, Dempster JM, Hahn WC, Vazquez F. The present and future of the Cancer Dependency Map. Nat Rev Cancer. 2025; 25: 59–73.

7. Xiao M, Yang J, Dong M, Mao X, Pan H, Lei Y, et al. NLRP4 renders pancreatic cancer resistant to olaparib through promotion of the DNA damage response and ROS-induced autophagy. Cell Death Dis. 2024; 15: 620.

8. Wang G, Cao J, Zhu Y, Wang S, Li Y, Yu Y, et al. Integrating Bulk RNA Sequencing and

CRISPR-Cas9 Screening to Identify Proliferation-Related Genes for Prognostic Stratification in Breast Cancer. J Cancer. 2025; 16: 2800–11.
9. Szambowska A, Tessmer I, Prus P, Schlott B, Pospiech H, Grosse F. Cdc45-induced loading of human RPA onto single-stranded DNA. Nucleic Acids Res. 2017; 45: 3217–30.
10. Huang J, Li Y, Lu Z, Che Y, Sun S, Mao S, et al. Analysis of functional hub genes identifies CDC45 as an oncogene in non-small cell lung cancer - a short report. Cell Oncol (Dordr). 2019; 42: 571–8.
11. Fu Y, Lv Z, Kong D, Fan Y, Dong B. High abundance of CDC45 inhibits cell proliferation through elevation of HSPA6. Cell Prolif. 2022; 55: e13257.
12. He Z, Wang X, Yang Z, Jiang Y, Li L, Wang X, et al. Expression and prognosis of CDC45 in cervical cancer based on the GEO database. PeerJ. 2021; 9: e12114.
13. Hu Y, Wang L, Li Z, Wan Z, Shao M, Wu S, et al. Potential Prognostic and Diagnostic Values of CDC6, CDC45, ORC6 and SNHG7 in Colorectal Cancer. Onco Targets Ther. 2019; 12: 11609–21.
14. Engebretsen S, Bohlin J. Statistical predictions with glmnet. Clin Epigenetics. 2019; 11: 123.
15. Wu T, Hu E, Xu S, Chen M, Guo P, Dai Z, et al. clusterProfiler 4.0: A universal enrichment tool for interpreting omics data. Innovation (Camb). 2021; 2: 100141.
16. Langfelder P, Horvath S. WGCNA: an R package for weighted correlation network analysis. BMC Bioinformatics. 2008; 9: 559.
17. Hashimoto Y, Sadano K, Miyata N, Ito H, Tanaka H. Novel role of DONSON in CMG helicase assembly during vertebrate DNA replication initiation. Embo j. 2023; 42: e114131.
18. Yang S, Ren X, Liang Y, Yan Y, Zhou Y, Hu J, et al. KNK437 restricts the growth and metastasis of colorectal cancer via targeting DNAJA1/CDC45 axis. Oncogene. 2020; 39: 249–61.
19. Li X, Abdel-Maksoud MA, Iqbal I, Mubarak A, Farrag MA, Haris M, et al. Deciphering cervical cancer-associated biomarkers by integrated multi-omics approach. Am J Transl Res. 2022; 14: 8843–61.
20. Wang S, Zhao Z, Yu L, Wang J, Ouyang Y, Zhou H, et al. Identification of Quercetin as a Natural MMP1 Inhibitor for Overcoming Cisplatin Resistance in Epithelial Ovarian Cancer. J Cancer. 2025; 16: 2578–94.
21. Wu L, Gao G, Mi H, Luo Z, Wang Z, Liu Y, et al. Validation of CDC45 as a novel biomarker for diagnosis and prognosis of gastric cancer. PeerJ. 2024; 12: e17130.
22. Guillerey C. NK Cells in the Tumor Microenvironment. Adv Exp Med Biol. 2020; 1273: 69–90.

Supplementary Files

This is a list of supplementary files associated with this preprint. Click to download.

- DU145cdc45ncsi123.png
- PC3cdc45ncsi123.png
- DU145gapncsi123.png
- PC3gapncsi123.png